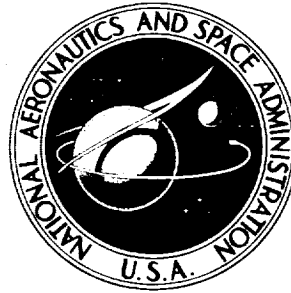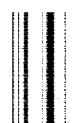NASA TECHNICAL NOTE

NASA TN D-2166

NASA TN D-2166

PREDICTION OF AERODYNAMIC PENALTIES CAUSED BY ICE FORMATIONS ON VARIOUS AIRFOILS

by Vernon H. Gray

Lewis Research Center
Cleveland, Ohio

NATIONAL AERONAUTICS AND SPACE ADMINISTRATION • WASHINGTON, D. C. • FEBRUARY 1964

PREDICTION OF AERODYNAMIC PENALTIES CAUSED BY

ICE FORMATIONS ON VARIOUS AIRFOILS

By Vernon H. Gray

Lewis Research Center
Cleveland, Ohio

NATIONAL AERONAUTICS AND SPACE ADMINISTRATION

PREDICTION OF AERODYNAMIC PENALTIES CAUSED BY

ICE FORMATIONS ON VARIOUS AIRFOILS[*]

SUMMARY

An empirical equation is developed by which changes in drag coefficients due to ice formations on an NACA 65A004 airfoil may be calculated from known icing and flight conditions; this equation is then extended to include available data for other airfoils with thickness ratios up to 15 percent. The correlation was obtained primarily by use of ice heights and ice angles measured on the 4-percent-thick airfoil. The final equation, however, does not include the ice measurements, but relates changes in drag coefficients due to ice with the following variables: icing time, airspeed, air temperature, liquid-water content, cloud-droplet-impingement efficiencies, airfoil chord, angles of attack, and leading-edge radius of curvature.

Changes in lift and pitching-moment coefficients due to ice on an NACA 0011 airfoil are also related to the corresponding changes in drag coefficients; additional data on lift and pitching-moment changes due to ice are limited to the 65A004 airfoil, for which complex trends preclude a general relation within the scope of this report.

INTRODUCTION

In the decade of the 1950's, much information about airfoil icing characteristics and the resultant aerodynamic penalties was acquired by the NACA. This information was obtained for the following airfoils shown in figure 1: 65A004, 63A009, 0011, 65_1-212, and 63_2-015. These airfoils have thickness ratios of 4 percent (ref. 1), 9 percent (ref. 2), 11 percent (ref. 3), 12 percent (ref. 4), and 15 percent (unpublished data), respectively. In addition, a much larger wealth of information concerning the cloud-droplet-impingement characteristics for a variety of airfoils and body shapes has been published. Unfortunately, despite these data, very little direct correlation has heretofore been shown between the aerodynamic penalties due to ice formations, the shape and location of

---

[*]The material contained herein was presented as a paper at the SAE National Aeronautic Meeting, Los Angeles, California, October 4, 1957, under the title "Correlation of Airfoil Ice Formations and Their Aerodynamic Effects with Impingement and Flight Conditions." It is now being published because of present interest in icing protection for light aircraft (CAR-3) and helicopters.

ice formations, and the impingement conditions that produce the ice. Impingement calculations do not quantitatively foretell the size or shape of ice that will form under given conditions, nor are the published aerodynamic penalties related to the actual ice size and shape except in a gross way. Furthermore, it is very difficult to estimate aerodynamic penalties in icing conditions different from those specifically investigated for a particular airfoil.

A review of the aerodynamic data from these previous icing studies showed that, to understand the effects of ice on airfoil characteristics, it would be necessary to study the exact ice shapes and sizes and to relate the aerodynamic effect of the ice to the known effects produced by surface roughness, flow spoilers, leading-edge flaps, etc., which ice simulates. Such a study was accomplished with icing data for the NACA 65A004 airfoil section shown in figure 1 (ref. 5). In this study, a variety of ice shapes was accurately measured and related to the generating impingement and icing conditions. The changes in airfoil drag coefficients due to ice were then correlated with the ice shapes and, finally, with impingement and flight conditions. The object of this report is to describe this analysis of icing data for the 4-percent-thick airfoil and to extend it to include all the airfoil sections for which aerodynamic data in NACA icing tunnel conditions are available.

This investigation was conducted in the NACA Lewis 6- by 9-foot icing tunnel over the following ranges of variables:

Airfoil thickness ratio, percent . . . . 4 to 15
Airfoil angle of attack, deg . . . . 0 to 12
Air velocity, mph . . . . up to 280
Air total temperature, $^\circ$F . . . . 0 to 30
Liquid-water content, g/cu m . . . . 0.25 to 2.0
Volume median droplet diameter, microns . . . . 7 to 19
Icing time, min . . . . up to 27
Pressure altitude, ft . . . . <3500

Increases in cloud liquid-water content were accompanied by increases in the droplet size because of the tunnel spray-system design.

ANALYSIS OF ICE SHAPE

The correlation of the aerodynamic effects of ice with its size and shape required accurate measurement of these factors. The measurements were made according to the following techniques. A typical photograph of the cross section of an ice formation at a 6° angle of attack is shown in figure 2. After an icing run, the ice on the airfoil was removed by a steam-heated ice scraper except for a narrow band in a chordwise plane normal to the surface. The camera was positioned near the airfoil leading edge and directed spanwise nearly parallel to the leading edge. A black 1/4-inch-mesh wire grid was placed against the ice to provide a scale of measurement, and a white wire of the screen was alined to be an extension of the airfoil chordline. A point plotting procedure was used with the photographs to obtain two-dimensional cross sections of the various ice formations (inset of fig. 2).

For purposes of analysis, all the cross sections of ice deposits on the 4-percent-thick airfoil section were reduced to two significant dimensions, h and θ, as shown in figure 3. Dimension h is the height of the edge of the ice first reached in going from the upper to the lower surface. The angle θ is measured between this ice edge and the extended chord line. The angle is positive if the ice edge is above the chord line and negative if the ice edge falls below the extended chord line.

Representation of ice formations by only these two dimensions ignores the part of the ice on the lower surface of the airfoil. Generally, however, protuberances on this region contribute very little drag to the airfoil, except near 0° angle of attack. In contrast, flow spoilers near the leading edge and toward the upper surface cause large drag increases.

It was found that the dimensions θ and h could each be empirically correlated with the icing test conditions. The resulting correlation for ice angle θ, measured primarily on the 4-percent-thick airfoil, is shown in figure 4. (Symbols are defined in the appendix.) In the abscissa of figure 4 the angle θ is modified by a term that accounts for the airfoil geometric angle of attack at which the ice was formed α_i. The ordinate is a parameter accounting for liquid-water content w, air total temperature t_0, and airfoil total droplet-impingement efficiency $\overline{E}_m$. Although considerable scatter of data points exists, the exponents and coefficients of the variables were each adjusted until an equal and minimum scattering of data about an average straight line was obtained.

A convenient scale for classifying the ice formations as rime or glaze ice is provided by figure 4. The point of demarcation between observed rime and glaze ice deposits lies approximately at a value of 32 on the abscissa scale. Ice formations that plot to the left of this point are progressively more rime-like and those to the right are progressively more glazelike. Thus, use of the ice-angle scale in reporting icing conditions or ice types should be more differentiating than use of the general terms rime and glaze.

The ice height h was correlated in a manner similar to that for the angle θ, and the result is shown in figure 5. The ice height h was found to vary approximately linearly with icing time τ and air velocity V_0. The term $\overline{\beta}_m$ in the icing parameter of figure 5 is the maximum local droplet-impingement efficiency for the airfoil and usually occurs very near the leading edge.

Although the correlations developed for θ and h in figures 4 and 5 were based on data for a 6-foot-chord NACA 65A004 airfoil, the relations agree remarkably well with limited unpublished icing data obtained on cylinders and struts of less than 1-inch chord size. Therefore, the correlations given for ice height and angle should be valid for a considerable range of airfoil shapes and sizes. Thus, with h and θ predictable, and provided airfoil impingement data are available for determining surface limits of impingement (e.g., see ref. 6), the aerodynamically significant features of an ice formation can be composed by calculation.

CORRELATION BETWEEN ICE SHAPE AND DRAG

Changes in drag coefficients due to ice formations on the 4-percent-thick

airfoil section were analyzed on the basis of the ice acting as a leading-edge flap or spoiler. A correlation was obtained utilizing the relations developed in figures 4 and 5 for θ and h, respectively. This correlation is shown in figure 6. The abscissa of figure 6 is the ice angle θ, as determined from the equation of the line given in figure 4. The ordinate of figure 6 is the change in drag coefficient caused by various ice formations corrected to a common height equal to 1 percent of chord $\Delta C_d c/100h$, where ΔC_d is the change in the drag coefficient from the clean airfoil value due to the addition of ice and c is the airfoil chord. As shown in the ordinate of figure 6, the dimension h is determined from the equation of the line given in figure 5; as a result, figure 6 now expresses the drag changes due to ice in terms that are either known or calculable in a design or flight performance study.

For clarity, the data points are not shown in figure 6, but instead, the mean curves that describe the trends. Included in the data are several cases in which ice was formed at an angle of attack α_i and the airfoil was then changed to an angle α, for which C_d was measured, and ΔC_d was obtained from the clean airfoil drag coefficient at angle α. These data alined themselves very well with the balance of the data taken at fixed angles of attack and thus corroborated the usefulness of θ in correlating ΔC_d.

Strikingly evident in figure 6 are the reductions in drag coefficients with ice on the airfoil at high angles of attack and low ice angles (rime icing). These drag reductions below the clean airfoil values are possible because of the high drag coefficients associated with flow separation from thin airfoils with sharp leading edges. The addition of rime ice at the higher angles of attack may at times add bluntness to the airfoil and form a drooped leading edge that assists the flow over the airfoil nose and reduces the amount of flow separation from the upper surface. Under glaze icing conditions, however, the ice acts as a flow spoiler and always increases the airfoil drag coefficients.

Changes in drag coefficients due to ice are shown in figure 6 for each of the geometric angles of attack investigated. An equation has been developed that agrees with the 4-percent-thick airfoil data of figure 6 and that accounts for variations in the angles of attack from 0° to 12°. This equation is as follows:

$$\Delta C_d \approx \left[8.7 \times 10^{-5}\, \frac{\tau V_0}{c}\, \sqrt{w \bar{\beta}_m}\, (32 - t_0)^{0.3} \right] \left(1 + 6 \left\{ (1 + 2\sin^4 12\alpha) \right.\right.$$

$$\left.\left. \sin^2\left[543\,\sqrt{w}\left(\frac{\bar{\bar{E}}_m}{32 - t_0}\right)^{1/3} - 81 + 65.3\left(\frac{1}{1.35^{\alpha_i}} - \frac{1}{1.35^{\alpha}}\right)\right] - 1.7\sin^4 11\alpha \right\}\right)$$

$$(1)$$

The term in the first bracket of equation (1) accounts for the height to chord

4

ratio of the significant ice formation, and terms in the last bracket account for the ice angle, the angle of attack, and the formation of ice at an angle of attack different from that under consideration. This last term vanishes when ice is formed at the same geometric angle of attack as that being considered ($\alpha_i = \alpha$). In the $\sin^2$ function in the last bracket of equation (1), the expression

$$543 \cdot \sqrt{w} \left(\frac{\overline{E}_m}{32 - t_0} \right)^{1/3} - 81 \quad \text{is valid between the limits 0 and 180; beyond these}$$

limits, a value of zero should be used for the expression instead of a calculated number.

PREDICTION OF DRAG CHANGES DUE TO ICE ON VARIOUS AIRFOILS

Because equation (1) for approximating the drag-coefficient changes due to ice on an NACA 65A004 airfoil was determined, it was desirable to attempt a similar relation for other airfoils, although ice measurements were available only for the 4-percent-thick airfoil. Accordingly, all the applicable NACA icing drag data from references 2 to 4 were inserted into equation (1) for trial, and impingement parameters were interpolated from data of reference 6. These icing data are listed in table I. It was found that an airfoil thickness trend appeared; to account for this trend, a factor r was introduced, which is the airfoil leading-edge radius of curvature in percent of chord. Also, in the absence of more knowledge as to the effect of sweep on drag due to ice formations, the 63A009 airfoil (sweep angle, 36°) was regarded for correlation purposes as an unswept two-dimensional airfoil, except that impingement, chord length, and radius of curvature were taken for the streamwise cross section of the airfoil.

A final equation was derived that represents the available icing drag data of the referenced airfoils and that is consistent with equation (1) for the 4-percent-thick airfoil:

$$\Delta C_d \approx \left[8.7 \times 10^{-5} \frac{\tau V_0}{c} \sqrt{w \overline{\beta}_m} (32 - t_0)^{0.3} \right] \left(1 + 6 \left\{ (1 + 2.52 \ r^{0.1} \sin^4 12\alpha) \right. \right.$$

$$\left. \left. \sin^2 \left[543 \ \sqrt{w} \left(\frac{\overline{E}_m}{32 - t_0} \right)^{1/3} - 81 + 65.3 \left(\frac{1}{1.35^{\alpha_i}} - \frac{1}{1.35^{\alpha}} \right) \right] - \frac{0.17}{r} \sin^4 11\alpha \right\} \right)$$

$$\tag{2}$$

Measured values of ΔC_d from table I and reference 5 are plotted in figure 7 against the values calculated by using equation (2). The order of agreement shown in figure 7 appears quite satisfactory, considering the nature and difficulty of obtaining aerodynamic, impingement, and meteorological data in icing conditions.

ESTIMATION OF LIFT AND PITCHING-MOMENT COEFFICIENTS

Unfortunately, changes in lift and pitching-moment coefficients due to ice formations are known only for NACA 0011 (ref. 3) and 65A004 (ref. 1) airfoils. In addition to these data, however, it should be possible to estimate changes in lift and moment coefficients by utilizing relations in the published aerodynamic characteristics of airfoils with and without flaps, spoilers, protuberances, etc.

From the limited data available in icing conditions, it appears that changes in lift and moment coefficients due to ice formations can be related to the concurrent changes in drag coefficients for a thick, blunt airfoil such as the 0011 airfoil, whereas no systematic relation is readily apparent for a thin, sharp-nosed airfoil such as the 65A004 airfoil. The relations between changes in lift, moment, and drag coefficients due to ice on the 0011 airfoil are shown in figure 8 as functions of geometric angle of attack (data of ref. 3). Well-established trends are evident in figure 8, wherein increases in drag coefficients are accompanied by similar increases in moment coefficients and by decreases in lift coefficients of generally larger magnitude. These trends are similar to the trends with the 65A004 airfoil, but only up to angles of attack of about 3°. At higher angles of attack, changes in lift and moment coefficients due to ice on the 4-percent-thick airfoil were erratic with respect to changes in drag coefficients, primarily because of the flow separation from the upper surface starting at an angle of attack of about 4° (ref. 1).

EXAMPLE OF USE OF CORRELATION

To illustrate how the preceding correlations may be used to assess the magnitudes of aerodynamic penalties for various airfoils in icing conditions, the following hypothetical icing encounters will be evaluated:

Flight and icing conditions	Icing encounter	
	A	B
Airfoil	65A004	65_1-212
Chord, in.	96	240
Angle of attack,[a] deg	2	2
Airspeed, mph	500	300
Pressure altitude, ft	8000	8000
Air total temperature, $^{\circ}$F	25	10
Liquid-water content, g/cu m	0.5	0.5
Volume median droplet diameter, microns	15	15
Duration in icing, min	4	7
Clean airfoil drag coefficient[a]	0.0067	0.0088

[a]Corresponding to tunnel geometric angle of attack (uncorrected).

From references 5 and 6 the following impingement parameters may be determined:

Parameter	Icing encounter	
	A	B
Modified inertia parameter, K_0	0.0179	0.00515
Maximum local droplet impingement efficiency, $\bar{\beta}_m$	0.67	0.35
Total droplet impingement efficiency, $\bar{E}_m$	0.18	0.033

Substitution of the preceding values in equation (2) yields the following:

	Icing encounter	
	A	B
Change in drag coefficient due to ice	0.0051	0.0008
Change from clean airfoil drag coefficient, percent increase	76	9

If the airfoil angle of attack is increased in a maneuver in clear air up to 8° with the ice formations that accumulated during the preceding encounters at 2^O angle of attack remaining where they were formed, the following results are obtained by use of equation (2):

	Icing encounter	
	A	B
Angle of attack at which ice was formed, deg	2	2
Angle of attack during clear air maneuver, deg	8	8
Change in drag coefficient due to ice	0.0127	0.0041
Clean airfoil drag coefficient (at 8°)	0.119	0.0127
Change from clean airfoil drag coefficient, percent increase	10.7	32.3

The 65_1-212 airfoil of encounter B is similar in shape to an NACA 0011 airfoil, so that the relations in figure 8 may be used to estimate the changes in lift and pitching-moment coefficients due to ice accumulated in icing encounter B. These changes were determined from the corresponding changes in drag coefficients previously enumerated and the ratio factors shown in figure 8. The following results were obtained:

	Angle of attack, deg	
	2	8
Change in lift coefficient	-0.0009	-0.023
Change in moment coefficient	0.0004	0.005
Clean airfoil lift coefficient (typical)	0.35	1.02
Clean airfoil moment coefficient (typical)	-0.035	-0.04
Change from clean airfoil lift coefficient, percent decrease	0.26	2.3
Change from clean airfoil moment coefficient, percent increase (less negative)	1.1	12.5

Changes in lift and pitching-moment coefficients due to ice formations on the 65A004 airfoil of encounter A are not obtainable from the present correlation, but must be estimated from data of reference 1 and related aerodynamic studies of leading-edge spoilers, flaps, etc.

The foregoing examples are typical of calculations that must be made for several representative icing encounters to assess fully the flight penalties due to ice and the need for ice-protection equipment.

CONCLUSIONS

It should be noted in conclusion that this correlation is a first-order approximation of the presently available aerodynamic and icing data for airfoils exposed to icing conditions in the NACA icing tunnel. Several factors that were thought to be secondary in importance were ignored in this analysis. The correlation should be useful, however, in estimating the type and size of ice formations that would result from any specified icing encounter, in estimating the aerodynamic penalties that would result from an encounter, and in making flight performance studies in which icing effects must be evaluated.

Lewis Research Center
    National Aeronautics and Space Administration
        Cleveland, Ohio, October 25, 1963

APPENDIX - SYMBOLS

C_d airfoil section drag coefficient

ΔC_d change in section drag coefficient due to ice

ΔC_l change in section lift coefficient due to ice

ΔC_m change in section pitching-moment coefficient (about the quarter-chord point) due to ice

c airfoil chord length, in.

$\overline{E}_m$ total droplet-impingement efficiency (see refs. 5 and 6)

h height of ice, in. (see fig. 3)

K_0 modified inertia parameter (see refs. 5 and 6)

r radius of curvature of airfoil leading edge, percent of chord

t_0 free-stream total air temperature, $^\circ$F

V_0 free-stream velocity, mph, or knots $\times$ 1.15

w liquid-water content of cloud, g/cu m

α airfoil geometric angle of attack (uncorrected for tunnel walls), deg

α_i airfoil geometric angle of attack at which ice deposit is formed (uncorrected for tunnel walls), deg

$\overline{\beta}_m$ maximum local droplet-impingement efficiency (see refs. 5 and 6)

θ ice angle, deg (see fig. 3)

τ icing time, min

REFERENCES

1. Gray, Vernon H., and von Glahn, Uwe H.: Aerodynamic Effects Caused by Icing of an Unswept NACA 65A004 Airfoil. NACA TN 4155, 1958.

2. von Glahn, Uwe H., and Gray, Vernon H.: Effect of Ice Formations on Section Drag of Swept NACA 63A-009 Airfoil with Partial-Span Leading-Edge Slat for Various Modes of Thermal Ice Protection. NACA RM E53J30, 1954.

3. Bowden, Dean T.: Effect of Pneumatic De-Icers and Ice Formations on Aerodynamic Characteristics of an Airfoil. NACA TN 3564, 1956.

4. Gray, Vernon H., and von Glahn, Uwe H.: Effect of Ice and Frost Formations on Drag of NACA 65_1-212 Airfoil for Various Modes of Thermal Ice Protection. NACA TN 2962, 1953.

5. Gray, Vernon H.: Correlations Among Ice Measurements, Impingement Rates, Icing Conditions and Drag Coefficients for an Unswept NACA 65A004 Airfoil. NACA TN 4151, 1958.

6. Gelder, Thomas F., Smyers, William H., Jr., and von Glahn, Uwe H.: Experimental Droplet Impingement on Several Two-Dimensional Airfoils with Thickness Ratios of 6 to 16 Percent. NACA TN 3839, 1956.

TABLE I. – AERODYNAMIC AND ICING DATA FOR FIVE AIRFOILS

NACA airfoil section	Chord length, c, in.	Radius of curvature, r, percent of chord	Sweep angle, deg	Angle of attack during icing, α_i, deg	Angle of attack, α, deg	Free-stream velocity, V_0, mph	Air total temperature, t_0, °F	Liquid-water content, w, g/cu m	Icing time, τ, min	Total droplet impingement efficiency, $\overline{E}_m$ (a)	Maximum local droplet impingement efficiency, β_m (a)	Change in drag coefficient due to ice, ΔC_d	Data from reference
65A004	72	0.10	0										1, 5
						(See refs. 1 and 5 for data)							
63A009	b82.8	0.63	36	2	2	260	25	0.83	15	0.079	0.46	0.0200	2
				4	4	260	25	.83	15	.073	.42	.0230	
				4	4	260	10	.55	15	.057	.38	.0075	
				4	4	260	25	.39	14	.051	.35	.0080	
0011	87.4	1.30	0	0	0	275	25	0.50	15	0.071	0.51	0.0137	3
				0	0	175	25	.50	16.3	.035	.39	.0038	
				0	0	275	10	.50	27	.072	.51	.0057	
				0	4	175	25	.50	16.3	.035	.39	.0140	
				2	2	275	25	.50	18	.067	.46	.0185	
				2	2	275	25	.70	12.5	.086	.53	.0178	
				2	2	275	10	.65	20	.079	.51	.0092	
				2	2	275	25	.30	18	.038	.35	.0022	
				2	6	175	25	.50	18	.036	.35	.0026	
				4	4	175	10	.50	18	.036	.35	.0096	
				4	4	275	25	.50	10.3	.065	.43	.0046	
				4	4	175	25	1.00	21	.071	.44	.0122	
				4	4	275	25	.50	15.5	.066	.43	.0119	
				6	6	175	25	1.00	12	.075	.43	.0190	
				8	8	175	20	1.00	12.5	.084	.49	.0345	
				8	8	175	25	1.00	8	.082	.47	.0236	
65₁-212	96	1.00	0	2	2	260	0	0.65	7	0.046	0.43	0.0004	4
				2	2	260	25	1.40	4	.074	.48	b.0042	
				2	8	260	25	1.40	5	.074	.48	c.0370	
				5	5	180	23	1.25	5	.064	.42	c.0034	
				5	5	260	25	.52	20	.043	.36	.0038	
				5	5	260	0	.70	10	.056	.40	.0017	
63₂-015	13	1.59	0	4	4	250	10	0.70	5	0.203	0.63	0.0090	Unpublished
				4	4	250	25	.50	10	.222	.66	.0830	

a Data interpolated from ref. 6.
b Streamwise direction.
c Cyclic deicing data.

11

Airfoil	Chord, in.
65A004	72
63A009	82.8 (36° Sweep angle)
0011	87.4
65_1-212	96
63_2-015	13

Figure 1. - NACA airfoil sections for which aerodynamic data in icing conditions are available. Scale, 1/20.
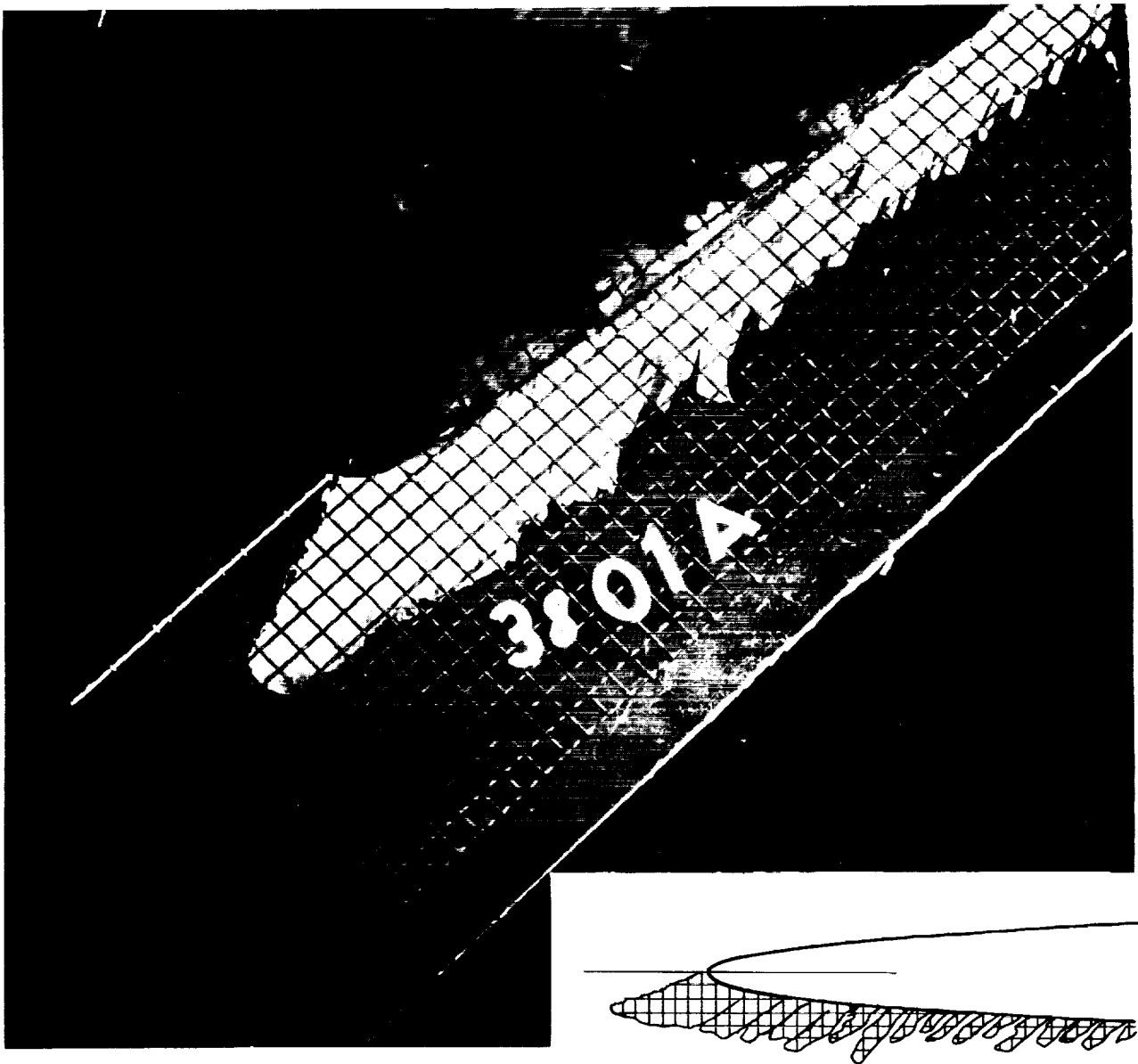
Figure 2. - Ice cross section and final two-dimensional sketch.
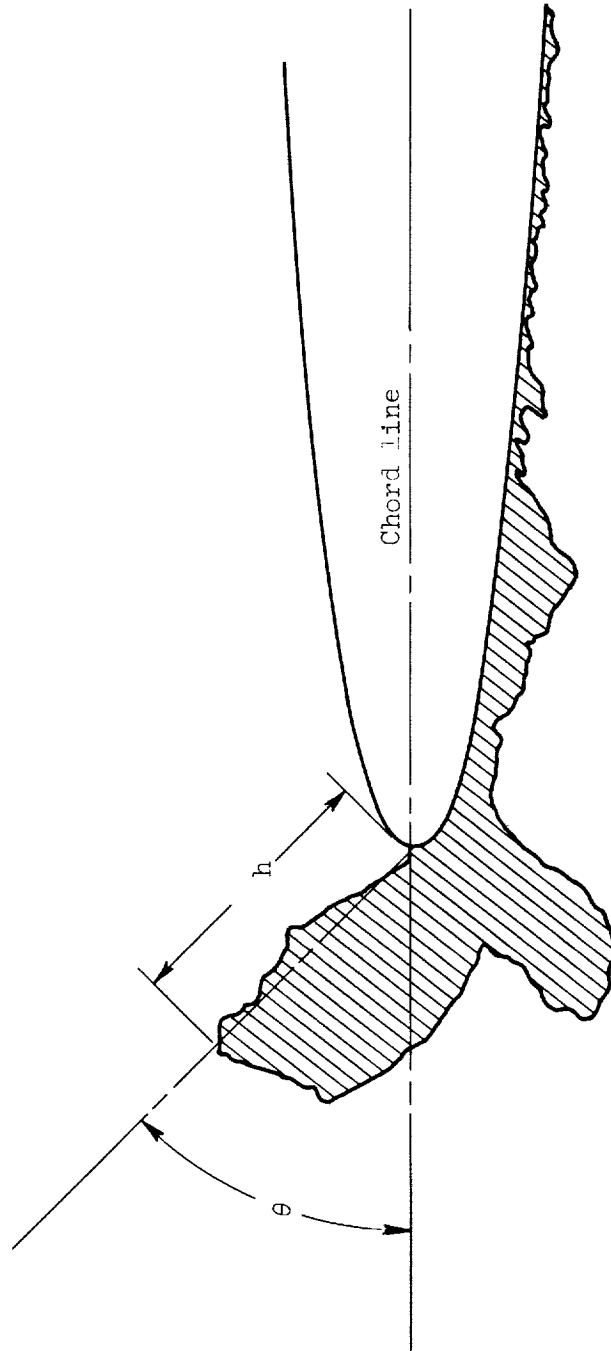
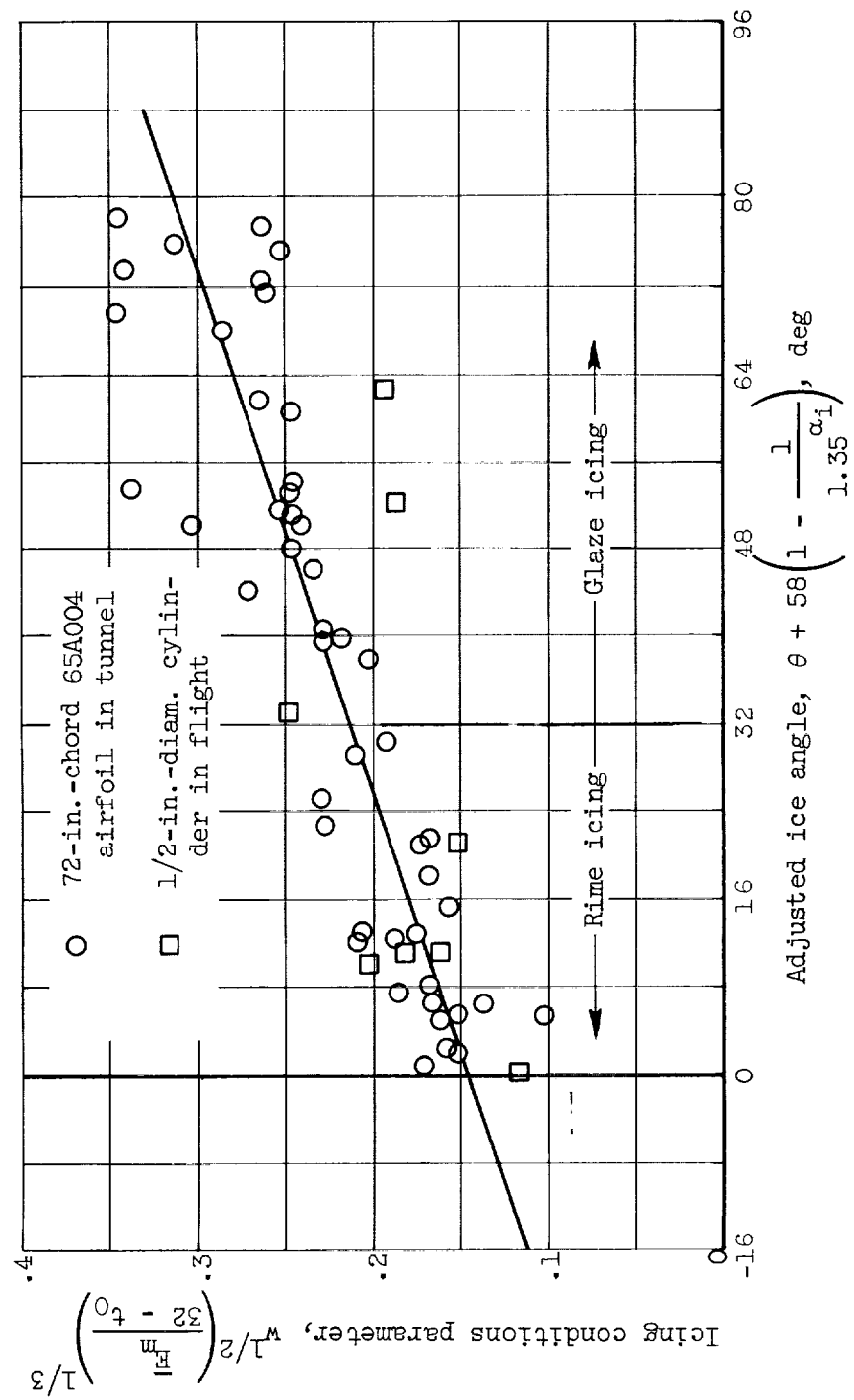Figure 3. - Representation of ice shape by angle θ and height h.

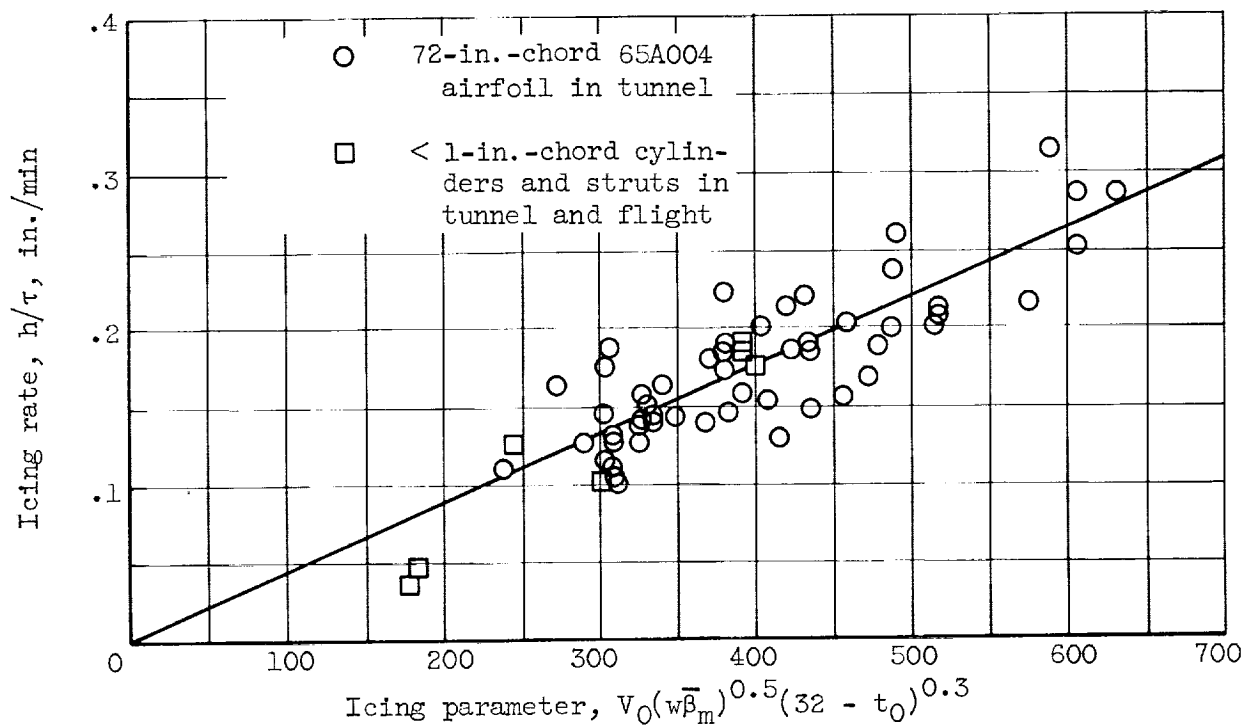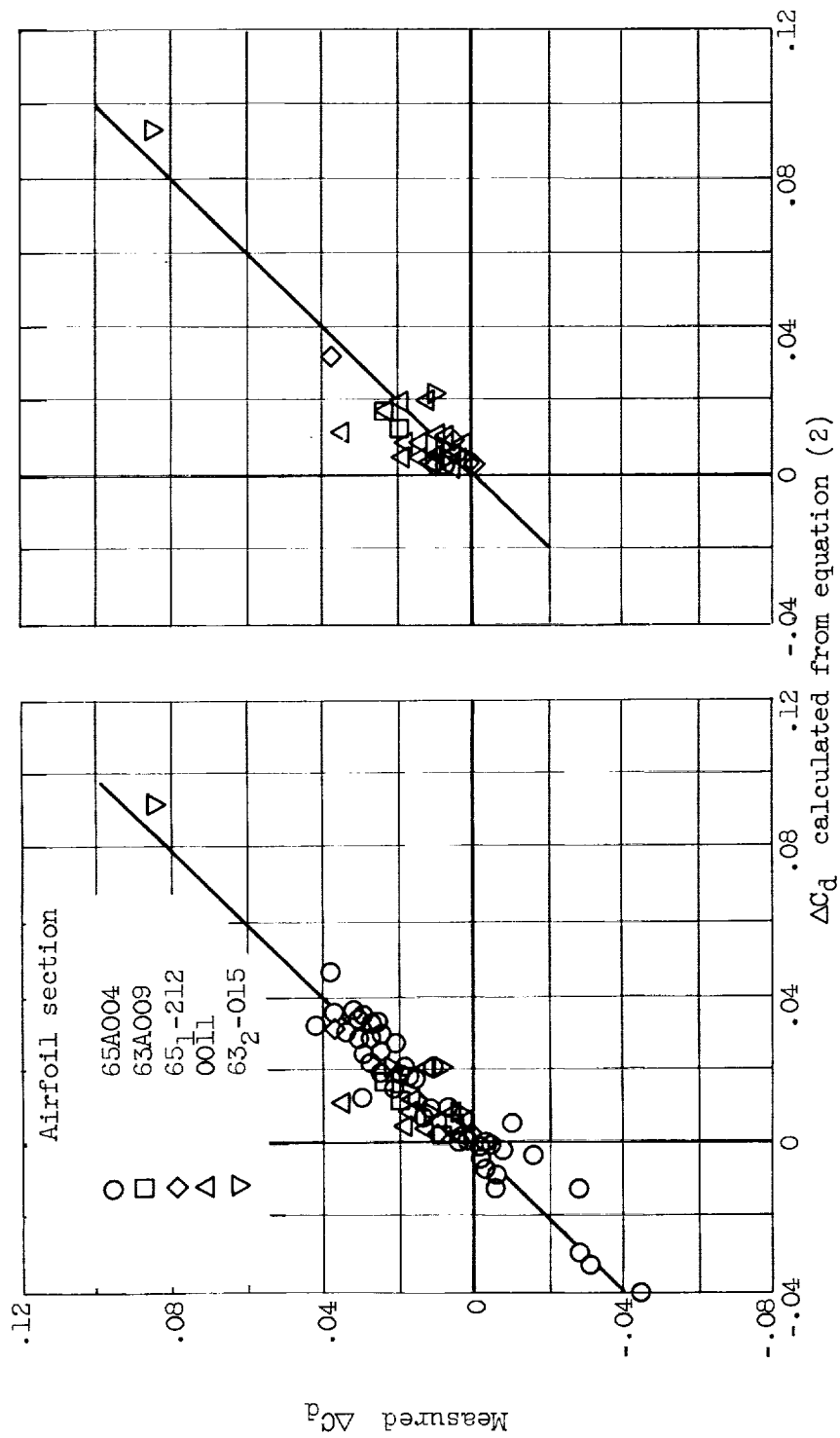Figure 4. - Correlation of ice angle with icing conditions.

The icing conditions parameter axis is labeled: Icing conditions parameter, $w^{1/2}\left(\dfrac{H_m}{32 - t_0}\right)^{1/3}$

The horizontal axis is labeled: Adjusted ice angle, $\theta + 58\left(1 - \dfrac{1}{\alpha_i^{1.35}}\right)$, deg

Legend:
○   72-in.-chord 65A004 airfoil in tunnel
□   1/2-in.-diam. cylinder in flight

Rime icing ←   → Glaze icing

15

Figure 5. - Correlation of ice height with icing conditions.

Figure 6. – Change in drag coefficient due to ice as function of ice angle and angle of attack.

17

(a) All available data.

(b) All available data except that for 65A004 airfoil.

Figure 7. - Comparison of calculated and measured change in drag coefficient due to ice, ΔC_d. (Complete range of NACA airfoil icing data.)
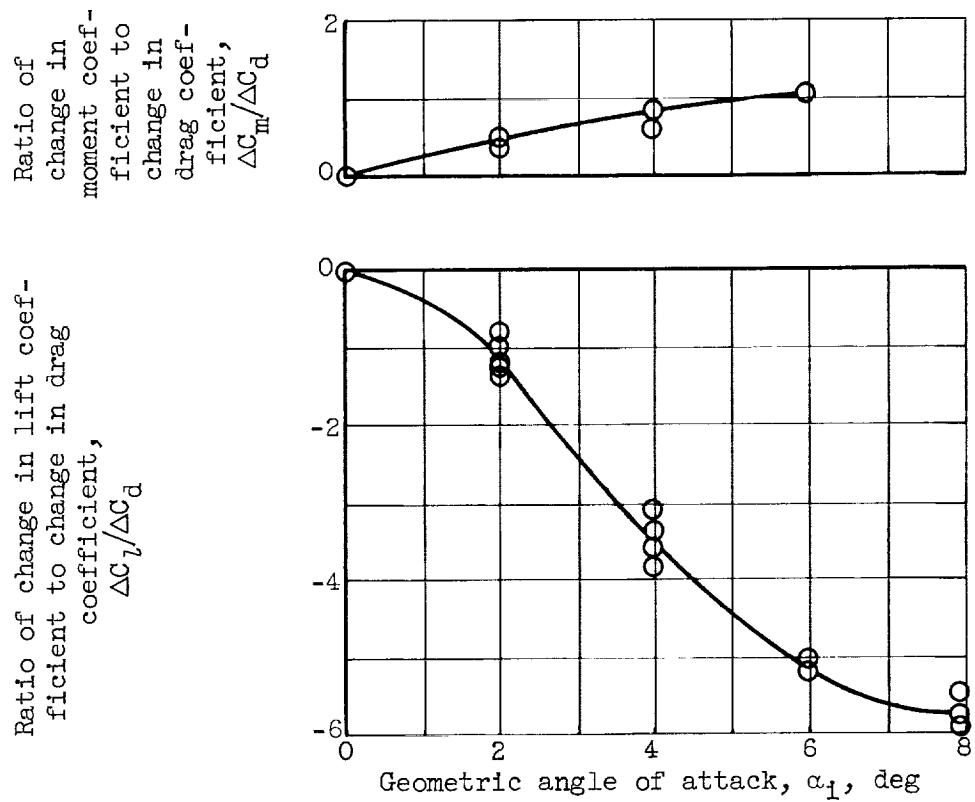
Figure 8. - Change in lift and pitching
moment due to ice on 0011 airfoil sec-
tion (related to change in drag).